Numerical study of 3D flow at right-angled confluences with and without upstream planform curvature

Dejana Đorđević

ABSTRACT

The purpose of this paper is to study the individual and combined effect of upstream planform curvature and difference in bed elevations at the tributary entrance to the confluence on the flow in the confluence hydrodynamics zone. To do this, flow at right-angled confluences with three planforms and four values of bed elevation discordance ratio ($\Delta z_T/h_d$) is simulated using a three-dimensional (3D) numerical model. Three confluence planforms include confluences with the (1) straight tributary canal (SC), (2) right bend (RB) and (3) left bend (LB) in the tributary. Four $\Delta z_T/h_d$ values in the range [0.0, 0.5] include both concordant and discordant beds' confluences. Overall, nine cases with the straight main canal are considered. Special attention is paid to the flow deflection and flow separation zones since the former affects transfer of momentum from the tributary to the main canal and the latter affects transport capacity of the post-confluence channel. Comparison of the results reveals that the influence of RB in the tributary is practically negligible in comparison to the straight canal case. With the increasing difference in bed elevations between the tributary and main canals (Δz_T), the presence of LB strengthens 3D flow and the structure of the recirculation zone is destroyed.

Key words | bed elevation discordance, 3D numerical modelling, river confluence, upstream planform curvature

Dejana Đorđević
Faculty of Civil Engineering,
University of Belgrade,
Bulevar kralja Aleksandra 73,
11000 Belgrade,
Serbia
E-mail: *dejana@grf.bg.ac.rs*

INTRODUCTION

A confluence hydrodynamics zone (CHZ) is a region within and near a river confluence with a three-dimensional (3D) fluid motion. Such a motion results from the collision between the combining flows and from their interaction with the riverbed. According to Best (Biron *et al.* 1996b), the CHZ consists of six distinct regions (Figure 1(b)): the flow stagnation, flow deflection, flow separation and flow recovery zones, the maximal velocity zone and two shear layers, one between the two combining flows and the other between the maximum velocity and flow separation zones. However, not all zones must be present at any particular confluence, since the existence, size and position of these zones is influenced by a number of factors. Until recently, it was considered that the major controls on flow in the CHZ were: (1) the confluence planform (in the sense of symmetry or asymmetry of the converging channels' directions with respect to the post-confluence channel direction); (2) the junction angle; (3) the momentum flux (or discharge) ratio of the confluent streams; and (4) the difference in bed elevations between the converging channels (bed elevation discordance). The role of these controls has been investigated during the last 20 years in laboratory confluences (Mosley 1976; Best & Reid 1984; Hager 1987, 1989; Ramamurthy *et al.* 1988; Weerakoon *et al.* 1990; Best & Roy 1991; Biron *et al.* 1996a, b; Gurram *et al.* 1997; Bradbrook *et al.* 1998; Hsu *et al.* 1998a, b; Shumate & Weber 1998) and field confluences (Biron *et al.* 1993; Gaudet & Roy 1995; Rhoads & Kenworthy 1995, 1998, 1999; Lane *et al.* 1998, 1999; De Serres *et al.* 1999; Rhoads & Sukhodolov 2001, 2004, 2008; Sukhodolov & Rhoads 2001), and by means of 2D (Lane *et al.* 1999) and 3D numerical models (Weerakoon & Tamai 1989; Bradbrook *et al.* 1998, 2000a, b, 2001; Lane *et al.* 1999, 2000; Huang *et al.* 2002; Biron *et al.* 2004; Đorđević & Ivetić 2006; Đorđević & Jovanović 2006;

doi: 10.2166/hydro.2012.150

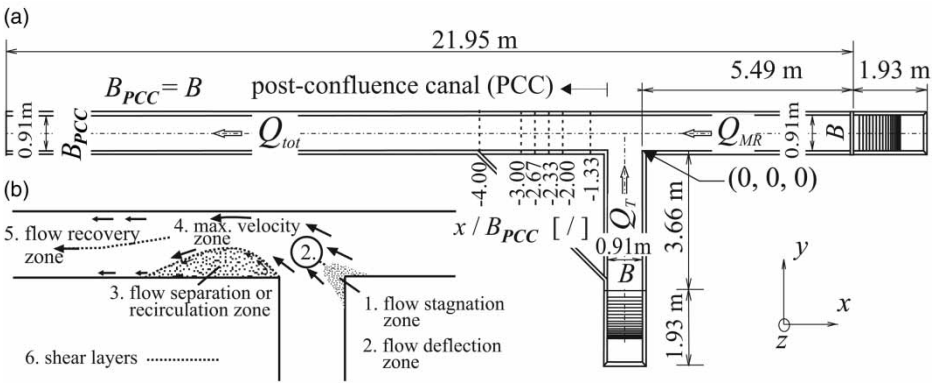

Figure 1 | (a) Plan view of the experimental setup of Shumate & Weber (1998); (b) description of the CHZ.

Đorđević & Biron 2008; Đorđević 2010a, b, 2012; Shakibainia *et al*. 2010). However, apart from being symmetrical or asymmetrical in the plan, river confluences in many cases also include planform curvature (one or both tributary stretches are curved). The problem is further complicated by the fact that the extensive field surveys revealed that difference in bed elevations between the upstream and downstream channels is rather a rule than an exception in the movable bed rivers (Biron *et al*. 1996b; Đorđević & Ivetić 2006; Đorđević & Jovanović 2006; Biron & Lane 2008; Đorđević 2010b). The role of upstream planform curvature was, indeed, recognised by Bradbrook *et al*. (2001) when trying to simulate numerically experiments in a single-flume confluence with a bend in the side canal of Biron *et al*. (1996a, b), but there was no attempt to investigate it either separately or in combination with other examined controls. Đorđević & Biron (2008) are the first ones who used these experiments to study (numerically) the effect of upstream planform curvature on the confluence hydrodynamics. At this point, it is worth noting that no flow separation zone and associated shear layer developed in these experiments, as the junction angle was rather small ($\alpha = 30^{\circ}$). Nevertheless, numerical simulations of 3D flow have shown that the presence of a bend in a tributary affects the flow in the flow deflection zone, where the exchange of momentum between the side and main canals takes place, and in the maximal velocity zone.

With such findings, it is interesting to study the effect of different bend orientations in a confluence that allows for the development of all six CHZ regions and consequently, depending on the findings, to study combined effect of an upstream bend and bed elevation discordance. To the author's knowledge, there are no laboratory investigations that could support this study. Thus, it was decided to use 3D numerical modelling as an alternative, cost-effective approach that would allow examination of a number of possible combinations of planform and riverbed geometries in the course of revealing whether the upstream planform curvature could be added to the existing list of controls. The study will proceed in three stages. In the first stage, which was the subject of the author's conference paper (Đorđević 2010a), only the effect of an upstream bend is investigated in the concordant beds' (CB) confluences. In the second stage, different degrees of bed elevation discordance between the main and tributary channels are studied in the straight channel confluences. Finally, in the third stage, the combined effects of the two geometrical features are studied in the discordant beds' (DB) confluences with a bend in the tributary.

A typical example of a confluence that allows for the development of all six CHZ regions is a CB' confluence with a 90° junction angle and sharp-edged corners as can be found in the laboratory experiments of Shumate & Weber (1998), where two straight laboratory canals of equal width and horizontal bed are joined together (Figure 1(a)). This confluence was used as a starting point for the analysis.

In the first stage, three planform geometries with the straight main canal are analysed: geometry with a straight tributary canal (SC), geometry with the right bend (RB) and geometry with the left bend (LB) in the tributary (Figures 2(a), 2(b) and 2(c)). In the RB case, the outer bank ends in the upstream junction corner, whereas in

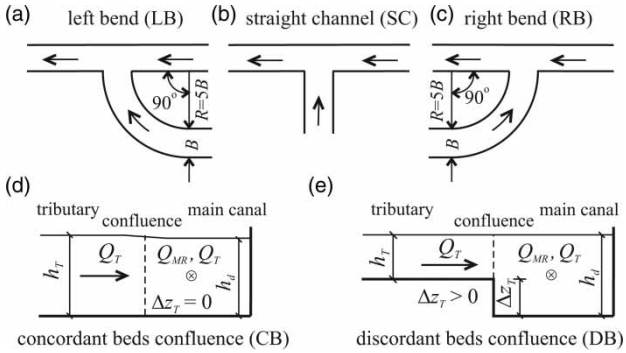

Figure 2 | Definition sketch for the three analysed confluence planforms and for the concordant and discordant beds confluences.

the LB case it ends in the downstream junction corner. Cross-sectional geometry of the two canals is the same as in the Shumate's laboratory confluence. The effect of different bend orientations on the flow deflection and flow separation zones is studied, as the former affects transfer of momentum from the tributary to the main canal, and the later one affects conveyance capacity of the post-confluence canal (PCC). The role of upstream bend is analysed by comparison of the (1) distributions of the flow angles along the junction lines at the tributary entrance to the confluence and (2) variations of the separation zone length and width throughout the flow depth, for the three geometries.

In the second stage, three additional hypothetical layouts of Shumate and Weber's (herein after Shumate's) straight canals' confluence are considered. These confluences have different values of the $\Delta z_T/h_d$ ratio, where Δz_T is the difference in bed elevations between the tributary and main canals, and h_d is the water depth in the main canal at the confluence. Together with the CB' SC confluence from the first stage ($\Delta z_T/h_d = 0.0$), this gives four $\Delta z_T/h_d$ values in the range [0.0, 0.5]. The value of 0.5 is the common value in field confluences (Biron & Lane 2008).

Based on the conclusions from the first stage, the effect of an upstream bend in the DB' confluences is studied only for the LB confluence, as the influence of the RB, when compared to the SC case, is practically negligible (Đorđević 2010a). Thus, in the last stage, three hypothetical layouts are considered again, this time with the LB in the tributary and three $\Delta z_T/h_d$ values in the range [0.1, 0.5].

Overall, there are nine distinct cases (Table 1) that should reveal how the upstream bend affects the flow field

Table 1 | Analysed combinations of the confluence planform and canal bed geometries

Case No.	$\Delta z_T/h_d$ [/]	R/B [/]	Bend orientation	Description
1	0.0	∞	/	CB' confluence of straight channels
2		5	Right	CB' confluence with a RB in the tributary
3		5	Left	CB' confluence with a LB in the tributary
4	0.10	∞	/	DB' confluence of straight channels
5	0.25			
6	0.50			
7	0.10	5	Left	DB' confluence with a LB in the tributary
8	0.25			
9	0.50			

in and downstream of the confluence, and finally, how the two controls interact. These answers are important for better understanding of physical processes at river confluences, such as mixing, erosion and deposition of sediments and pollutants, as river confluences have a prominent role in the drainage of a catchment, conveyance of sediments, and transport and mixing of pollutants.

NUMERICAL MODEL

In this study, the SSIIM2 model, developed by Olsen (2000), is used. This is a 3D finite-volume model that solves the Reynolds-averaged Navier-Stokes (RANS) equations for the incompressible fluid flow. The Reynolds stresses from these equations are modelled with the Boussinesq model in which the unknown eddy viscosity coefficient is related to the turbulence kinetic energy (TKE) k and its dissipation rate ε via expression: $\nu_t = c_\mu k^2/\varepsilon$, i.e., the k-ε type two-equation turbulence model closure is used. Although there are two types of the k-ε model available in SSIIM2, the standard k-ε model and the RNG (ReNormalisation Group) k-ε model of Yakhot *et al.* (1992), the standard k-ε model is used as it provided better agreement with measurements (Đorđević in preparation). The values of the model parameters in the standard k-ε model are: $c_\mu = 0.09$, $\sigma_k = 1.00$, $\sigma_\varepsilon = 1.30$, $C_{1\varepsilon} = 1.44$ and $C_{2\varepsilon} = 1.92$.

The equations are solved on the 3D orthogonal or non-orthogonal unstructured multi-block grid, as this type of grid allows for simulations in dendritic flow domains that are characteristic for river confluences. The SIMPLE algorithm is used for coupling the mass and momentum equations. Convective terms in the momentum equations can be discretised either with the first- or the second-order upwind scheme (FOU or SOU).

In subcritical flow, known discharges are prescribed at inflow boundaries and constant depth is prescribed at the outflow boundary. The k and ε values at inflow boundaries are subsequently determined based on the known vertical eddy viscosity distribution and the assumptions on the equilibrium of the production and dissipation of TKE near the solid boundary, and linear vertical variation of the TKE, with the surface k-value equal to half the bottom value (Olsen 2000). The solid boundaries are treated with the wall-law and the symmetric boundary conditions are used for calculation of the velocities at the outflow and free-surface boundaries, with the exception of the vertical velocity that is set to zero at the free-surface. Though there are models that use porosity approach to define position of the free-surface, in the SSIIM2 model, the free-surface is approximated with the rigid lid, i.e., the position of the free-surface is not explicitly modelled. However, it can be determined from the calculated pressure field, using the hydrostatic pressure distribution assumption.

MODEL VALIDATION

The SSIIM2 model has been tested and validated against various experimental and field data. A list of applications is long. Thus, only a selection is cited here. Olsen (2003) and Rüther & Olsen (2006) tested the model with data collected in a meandering laboratory canal, Viscardi *et al.* (2006) validated the model with the field data from the Parana River tributary, Đorđević & Biron (2008) tested the model against single-flume confluence data, Stoesser *et al.* (2010) against the experimental data from the 180° canal bend and Shakibainia *et al.* (2010) against 90° laboratory confluence data.

For this study, only experimental data from the Shumate's 90° open-channel junction are relevant. Thus, only a selection of the results from Đorđević (in preparation) is given here. Layout of the right-angled CB' confluence is presented in Figure 1(a). A series of six experiments with unaltered total discharge of 0.17 m^3/s and downstream flow depth of 0.296 m, giving the $Fr = 0.37$ and $Re = 185{,}888$, was conducted in this facility. Values of the discharge ratio between the upstream main canal discharge and the total combined discharge ranged between 0.083 and 0.917. The flow was steady and subcritical in all experiments. The three velocity components (u, v, w) were measured with the acoustic Doppler velocimeter (ADV) in 2,850 points in each experiment. The length and width of the separation (recirculation) zone was not measured. Details of the experimental procedure can be found in Shumate & Weber (1998). It is worth noting that the downstream cross-section of the side-canal was densely covered with measurements. This allowed the author to assess the model's ability to transfer the momentum from the tributary correctly during the model validation procedure (Đorđević 2010b, in preparation).

The experiment in which a large, visible recirculation zone (RZ) was formed downstream of the confluence was chosen for this study. The upstream main canal and side canal discharges in this experiment were $Q_{MR} = 0.099\ m^3/s$ and $Q_L = 0.071\ m^3/s$, giving the discharge ratio value of $Q_{MR}/Q_{tot} = 0.583$.

Each of the two canals in Figure 1(a) was covered with the 3D orthogonal structured grid (or a block). The main and post-confluence canals were covered with block 1 and the tributary canal with block 2. Three grid densities were used in the grid sensitivity analysis. The grids are listed in the decreasing grid density order: (1) grid 1: $838 \times 37 \times 20$ (block 1) and $182 \times 37 \times 20$ (block 2); (2) grid 2: $440 \times 19 \times 10$ (block 1) and $91 \times 19 \times 10$ (block 2); and (3) grid 3: $313 \times 13 \times 10$ (block 1) and $65 \times 13 \times 10$ (block 2). The three digits stand for the number of cells in the stream-wise, lateral and vertical directions, respectively. Both FOU and SOU schemes were used for discretisation of the convective terms in the momentum equations with the finest grid. The presented results refer to the SOU scheme if not otherwise indicated.

Calculated and measured velocities (u, v, w) and k for the finest and the coarsest grids are compared in Figures 3–6. It can be noticed that there are no significant differences between the two grids for the u and v velocities (Figures 3 and 4; the linear regression line slopes for the u and v are 0.99 and

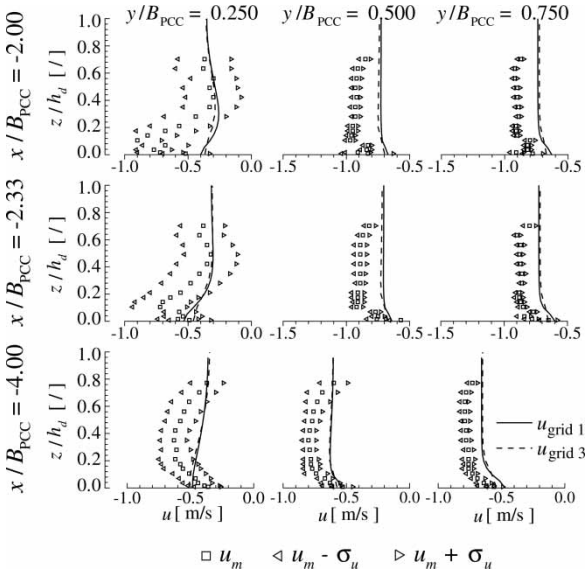

Figure 3 | Comparison of the calculated and measured stream-wise velocity profiles in three cross-sections downstream of the confluence.

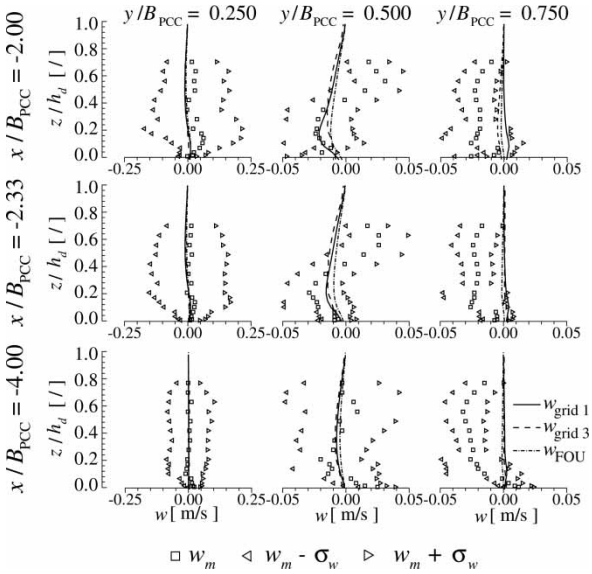

Figure 5 | Comparison of the calculated and measured vertical velocity profiles in three cross-sections downstream of the confluence.

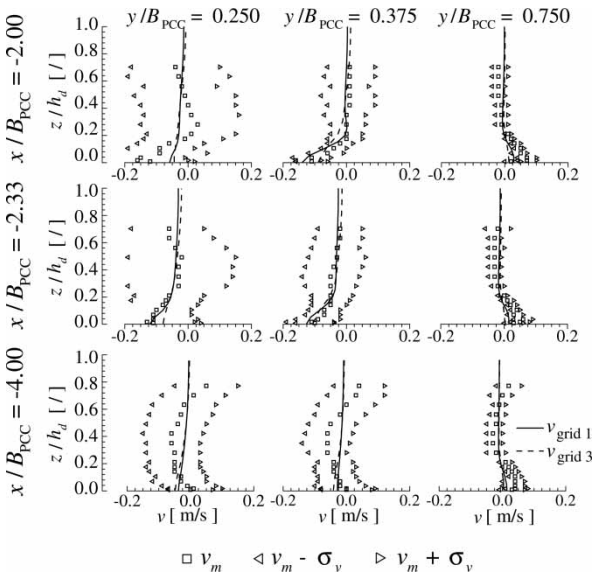

Figure 4 | Comparison of the calculated and measured lateral velocity profiles in three cross-sections downstream of the confluence.

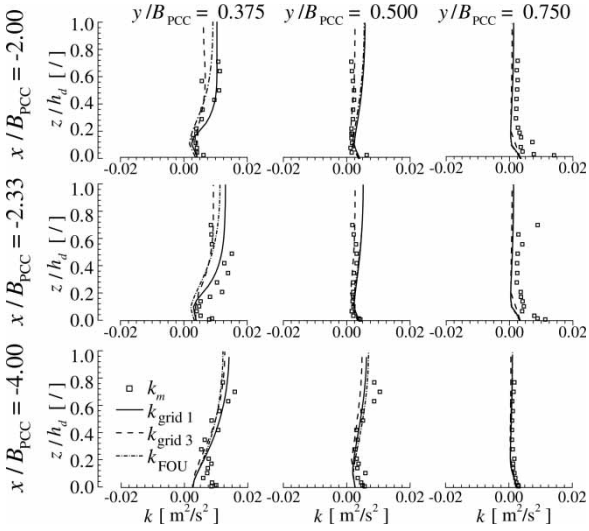

Figure 6 | Comparison of the calculated and measured profiles of the TKE in three cross-sections downstream of the confluence.

1.03, and the corresponding correlation coefficients $\rho_u = \rho_v = 0.99$). The differences are apparent for the w-velocity and k in the RZ area (Figures 5 and 6, $x/B_{PCC} = \{-2.00, -2.33\}$, see Figure 1(a)), where $\rho_w = 0.63$ and $\rho_k = 0.36$.

The shape of the u-velocity profiles is captured well (Figure 3). Moreover, calculated profiles in the RZ are in the space bounded by the measurement errors. However, the velocity magnitudes outside the RZ are underpredicted by 15–17%. This difference is expected because the free-surface is presented with the rigid lid. Almost perfect matching of the calculated and measured v-velocity profiles in the shear layer (Figure 4, $y/B_{PCC} = 0.375$) means that the model describes correctly extraction of the momentum

from the main flow to the RZ. Outside the RZ, v-velocity magnitudes are underpredicted by the same amount as u-velocities. Vertical velocity magnitudes are underpredicted by almost 50%. It is believed that such a large discrepancy results both from the rigid lid and hydrostatic pressure distribution assumptions. It is worth noting that neither Huang *et al.* (2002) nor Shakibainia *et al.* (2010) reported results for the w-velocity and k.

The difference between FOU and SOU schemes becomes apparent when plotting the vertical variation of the RZ dimensions (Figure 7). The length and width were read from the streamline plots for the calculated and measured velocity fields. In estimating the 'measured' RZ length, streamlines of the measured velocity field were extrapolated to the wall since the first measuring vertical had been placed 5 cm from the junction-side wall (Figure 7(c)). Thus, the measured L_{RZ} should be taken only as a rough estimate of the true length. The streamline 'candidates' for extrapolation were selected visually. There were usually three candidates. The differences in readings $(L_{m3} - L_{m1})$ are $0.08B_{PCC}$ on the average, and the standard deviation is $0.02B_{PCC}$. Only L_{m3} readings are presented in Figure 7(a). The results undoubtedly show superiority of the SOU over the FOU scheme (discrepancies for the SOU scheme are ±5% and for the FOU scheme, between 16 and 26%).

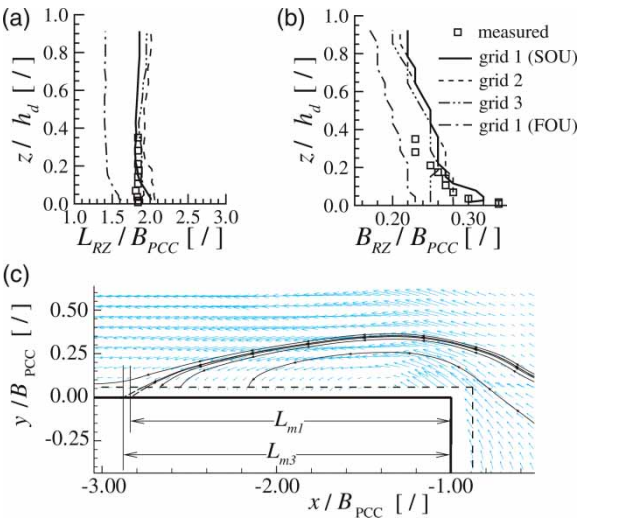

Figure 7 | (a) and (b) Comparison of the calculated and 'measured' RZ dimensions; (c) procedure for estimation of the measured RZ length.

NUMERICAL STUDY OF RIGHT-ANGLED CONFLUENCES

Numerical modelling details

The three investigated planform geometries are shown in Figures 2(a), 2(b) and 2(c). The SC case corresponds to the geometry presented in Figure 1(a). In the LB and RB cases, the SC is replaced with the curved one having the radius of curvature $R = 5B$ (B is the width of the tributary) and the central angle of 90°. The computational grid in the RB and LB cases also consists of two blocks, the only difference to the SC case being the fact that the grid in block 2 is curvilinear because of the presence of the bend. While the upstream boundary in the tributary canal for the SC case coincides with the end of the corresponding canal in the Shumate's facility, the upstream boundary in the curved tributary is placed five canal widths upstream of the bend. The upstream and downstream boundaries of the main canal coincide with the inflow and outflow cross-sections in the Shumate's facility. Such positioning of the computational domain boundaries ensured no influence thereof on the flow pattern in the CHZ.

The two blocks have the same number of cells in the vertical direction in the CB' confluences (Figure 2(d)). In the DB' confluences (Figure 2(e)), the number of cells in the tributary block reduces with the increase in the $\Delta z_T/h_d$ value. The size of block 1 is the same for all confluence layouts. The nine cases considered are listed in Table 1.

Both the upstream planform curvature and bed elevation discordance were accounted for in the grid sensitivity analysis. Four cases from Table 1 were chosen for analysis 1, 3, 6 and 9. The sizes of block 1 are already listed in the section Model validation. The considered sizes of block 2 in the left bend CB' confluences were: (1) $480 \times 37 \times 20$ for grid 1; (2) $341 \times 19 \times 10$ for grid 2; and (3) $234 \times 13 \times 10$ for grid 3. In the corresponding DB' confluences with $\Delta z_T/h_d = 0.50$, the number of cells along the vertical was halved.

Due to very small differences in the results between the three grids, it was not possible to assess numerical uncertainty using the GCI (grid convergence index) method in its full form as defined by Celik *et al.* (2008), i.e., the apparent

order of accuracy could not have been calculated in many cross-sectional points. Therefore, the GCI method was applied using the formal order of accuracy of the numerical scheme ($p = 2$). The *GCI*-values averaged over the cross-section $x/B_{PCC} = -2.00$ for grids 1 and 2 ($\overline{GCI}_{21}$) and for grids 2 and 3 ($\overline{GCI}_{32}$) are given in Table 2 for the four considered cases. The cross-sectional distributions for the five variables (u, v, w, k, ε) are presented for illustration only for case 9 (Figure 8). The GCI_{21}-values (for the finest grid) are below 5% in the substantial part of the cross-section for all five variables in cases 1, 3 and 6. In case 9, they are below 10 and 15% for (u, w, k, ε) and v, respectively. Thus, the following block sizes were accepted in CB' confluences: $838 \times 37 \times 20$ (block 1), $182 \times 37 \times 20$ (block 2) for straight canal and $480 \times 37 \times 20$ (block 2) for LB and RB confluences. The size of block 2 in the vertical direction in DB' confluences decreased depending on the extent of bed elevation discordance. The vertical number of cells was 18, 15 and 10 for $\Delta z_T / h_d = \{0.10, 0.25. 0.50\}$, respectively.

RESULTS AND DISCUSSION

Individual and combined effects of the two geometrical features are investigated in the same fashion. The investigation starts with the study of flow deflection in both horizontal and vertical planes at the tributary entrance to the confluence, where the CHZ begins. The measure of flow deflection in the horizontal plane is the flow angle $\delta = \text{arc tg}(v/u)$, and the measure of flow deflection in the vertical plane, i.e., the measure of the strength of 3D flow, is the flow angle $\varphi = \text{arc tg}\left(w/\sqrt{u^2 + v^2}\right)$. Consequently, variations of the RZ length and maximal width in the vertical direction, the resulting changes in the position and shape of the shear layer that develops between the recirculation and maximal velocity zones, and k-distributions are considered.

Effect of upstream planform curvature

Flow angles

Distributions of the two angles along the lines that are connecting upstream and downstream junction corners at several elevations above the canal bed are presented in Figure 9. It can be noticed that the influence of the RB is almost negligible, i.e., distributions of both angles for the SC and RB cases are nearly identical except close to the bottom where δ-angle value is exceeded by 30–50% when there is a bend in a tributary (Figure 9(a), $z/h_T = 0.008$). Small differences in the δ- and φ-angle values reflect the influence of the centrifugal force resulting from the planform curvature. In the RB case, centrifugal forces due to planform curvature and abrupt change in the tributary flow direction act in the same direction, hence the small shift of the δ- and φ-lines. In the LB case, the two centrifugal forces act in the opposite directions and there is remarkable difference in both δ- and φ-angle distributions when compared to the SC and RB cases. Close to the bottom ($z/h_T < 0.100$), where velocities are lower, centrifugal force from the RB helps the flow from the main canal to turn the tributary flow in the main canal direction, while in the LB case, centrifugal force from the LB helps the flow to keep its original direction. Therefore, there is much greater deflection of the δ-angle from the junction angle α in the SC and RB cases than in the LB case (Figure 9(a),

Table 2 | Averaged cross-sectional *GCI* values in the cross-section $x/B_{PCC} = -2.00$ for cases 1, 3, 6 and 9

	Case 1		Case 6		Case 3		Case 9	
	$\overline{GCI}_{32}$	$\overline{GCI}_{21}$	$\overline{GCI}_{32}$	$\overline{GCI}_{21}$	$\overline{GCI}_{32}$	$\overline{GCI}_{21}$	$\overline{GCI}_{32}$	$\overline{GCI}_{21}$
u	4.00	0.24	1.75	0.22	3.14	0.9	1.73	0.44
v	20.30	1.51	9.12	1.43	23.68	2.15	25.20	16.58
w	23.24	2.26	9.02	1.22	17.85	2.43	21.84	7.48
k	8.26	0.81	5.53	0.72	6.3	0.76	4.92	2.29
ε	11.96	1.93	8.28	1.7	7.62	1.86	9.03	4.41

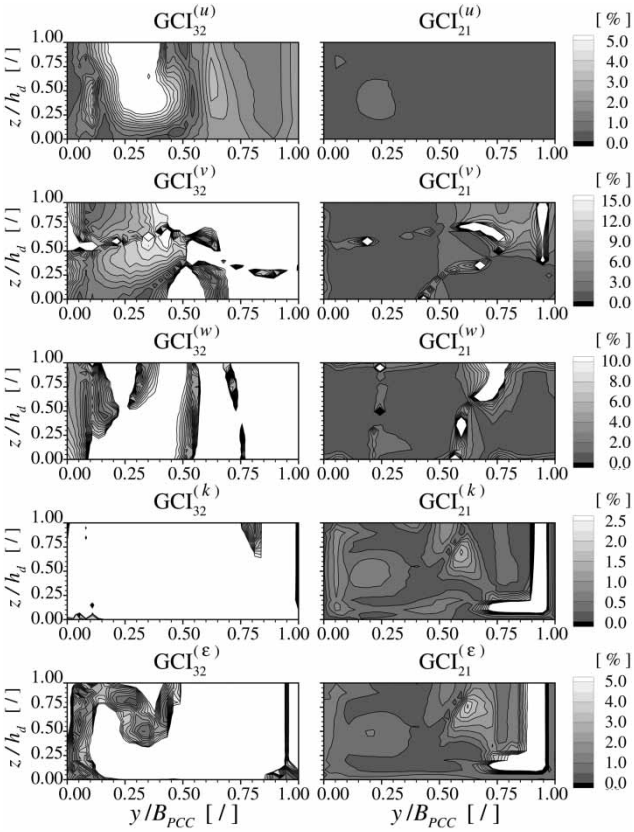

Figure 8 | Distributions of grid convergence indices GCI_{32} and GCI_{21} for three velocity components (u, v, w), k and ε in the cross-section $x/B_{PCC} = -2.00$ for the DB′ confluence with the LB in the tributary (case 9 from Table 1).

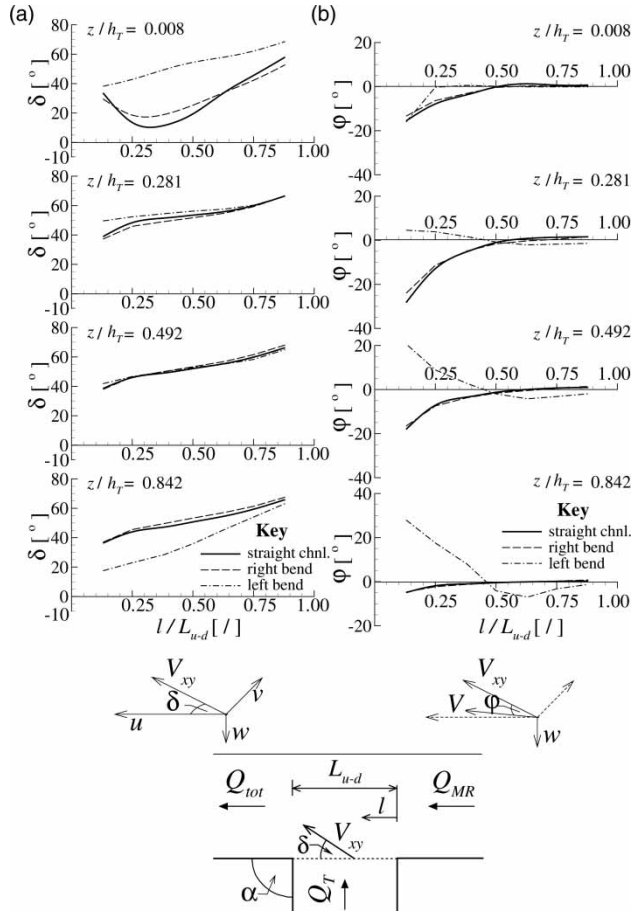

Figure 9 | Effect of upstream planform curvature on the variation of flow angles: (a) δ and (b) φ along the junction line at different elevations above the canal bed.

$z/h_T = 0.008$). The dominance of the centrifugal force from the LB over the centrifugal force due to change in the tributary flow direction gradually diminishes by $z/h_T \approx 0.500$, where δ-angle distributions for the three cases overlap. From this level to the water surface, the flow from the LB starts turning more rapidly under the influence of the main canal flow, which is much faster (stronger) than it is in the bottom layers. Distributions of the φ-angle (Figure 9(b)) indicate that in the LB case the flow deflects in the opposite direction to that in the SC and RB cases. Close to the upstream junction corner, φ-angle is positive, meaning that the streamlines are directed to the water surface, while in the SC and RB cases, φ-angle is negative suggesting that the flow is directed to the bottom. At the downstream junction corner the situation is the reverse to that at the upstream corner. However, φ-angle values are reduced almost to zero indicating that there is no significant deflection of flow in the vertical plane.

Recirculation zone

RZ length and maximal width at different elevations above the bed were estimated from the streamline plots (Figures 10(a), 10(b) and 10(c)). Their variations throughout the water column are presented in Figures 10(d) and 10(e). Both the RZ length and width reduce with distance from the bottom no matter whether the tributary is curved or straight. It can be noticed that the RZ length reduces faster in the LB case than in the SC and RB cases (Figure 10(d)). This can be explained by the change in dominance between the two centrifugal forces of the opposite directions. Close to the bottom, where centrifugal force due to planform curvature dominates, the RZ is 15% longer than the one that forms when the tributary canal is straight and 5% shorter than that resulting from right-bend tributary flow. In the upper layers

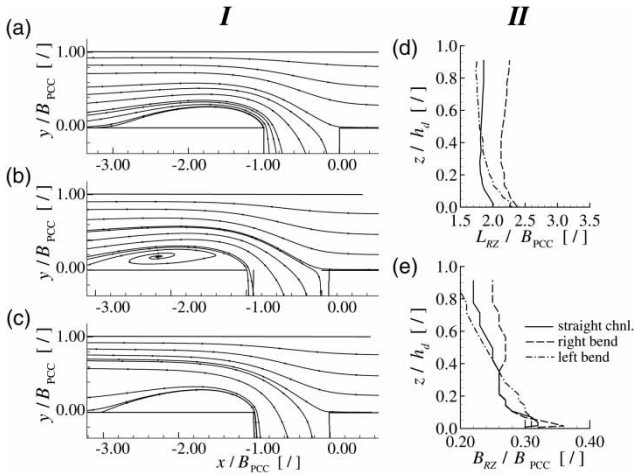

Figure 10 | Effect of upstream planform curvature on the RZ dimensions. I: Streamlines that bound RZ at $z/h = 0.069$ for the confluence with the (a) SC, (b) RB in the tributary and (c) LB in the tributary. II: Variations of (d) non-dimensional RZ length and (e) non-dimensional RZ width.

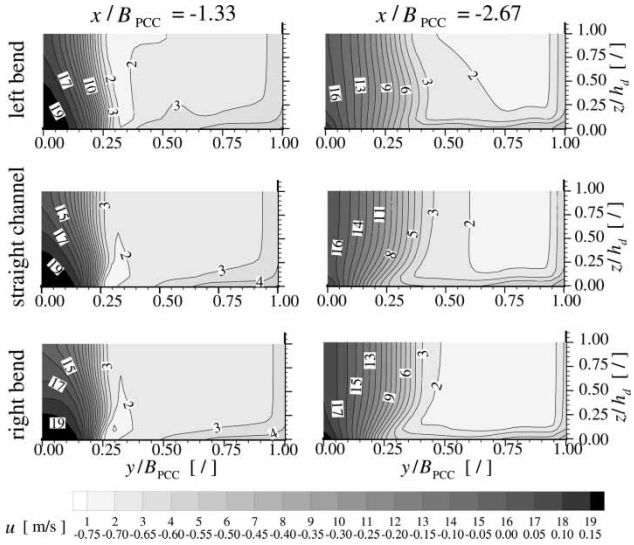

Figure 11 | Effect of upstream planform curvature on the cross-sectional stream-wise velocity distributions downstream of the confluence. (Cross-sections are indicated in Figure 1.)

($z/h_d > 0.70$), where centrifugal force due to change in the tributary flow direction dominates, the RZ is 5% shorter than that in the SC case and 25% than that in the RB case. Superposition of the two centrifugal forces of the same direction in the RB case results in a consistent increase in the RZ length by 20% when compared to that from the SC case.

In the upper layers, variations of the RZ width show similar tendencies to those observed with the RZ length – the widest RZ is formed in the RB case and the narrowest in the LB case (Figure 10(e)). The RZ width is increased by 15% in comparison to the SC case when there is a RB in the tributary, and it is reduced by 8% in the LB case. This is in accordance with the δ-angle distributions from Figure 9, where the least deflection from the junction angle (α-δ) is observed in the RB case and the greatest in the LB case. Below $0.35h_d$ the situation is quite the opposite – for the confluences with a LB in the tributary, RZ is up to 10% wider than that in the SC and RB cases.

Change in the RZ width with distance from the bed is also visible on the cross-sectional distributions of the stream-wise velocity u (Figure 11, $x/B_{PCC} = -1.33$). Here, one can see the differences in the position of the shear layer and shear intensities for the three planforms. In the LB case, shear layer is inclined towards the junction sidewall at an almost constant angle throughout the flow depth, while in the SC and RB cases it is curved towards the opposite wall. The maximal curvature is attained at $0.30h_d$ in the SC case and between 0.35 and $0.40\,h_d$ in the RB case. The greatest shear between the RZ and the zone of maximal velocities is developed in the bottom 0.25–0.30 h_d regardless of the confluence planform type (with or without a bend). The wider RZ in the LB case produces lower shear than the narrower RZ in the SC and RB cases. For example, at $x/B_{PCC} = -1.33$, the shear ($\Delta u/\Delta y$) is approximately 13% lower than that for the SC case. On the other hand, the presence of the RB increases the shear – at $x/B_{PCC} = -1.33$ the increase is around 5%, which is practically negligible.

The variable shape of the RZ affects the zone of maximal velocities. When the RZ is wider (LB case) the core of maximal velocities is larger and it extends throughout the flow depth, while in the SC and RB cases, the core is located in the lower part of the water column (Figure 11, $x/B_{PCC} = -1.33$). As can be seen, the effect of different bend orientations on the core of maximal velocities extends downstream of the RZ (Figure 11, $x/B_{PCC} \leq -2.67$), i.e., in the LB case the core is inclined towards the junction sidewall far downstream of the confluence.

TKE

TKE distributions in the cross-section $x/B_{PCC} = -1.33$ are presented in Figure 12 ($\Delta z_T/h_d = 0.00$). The RB and LB in

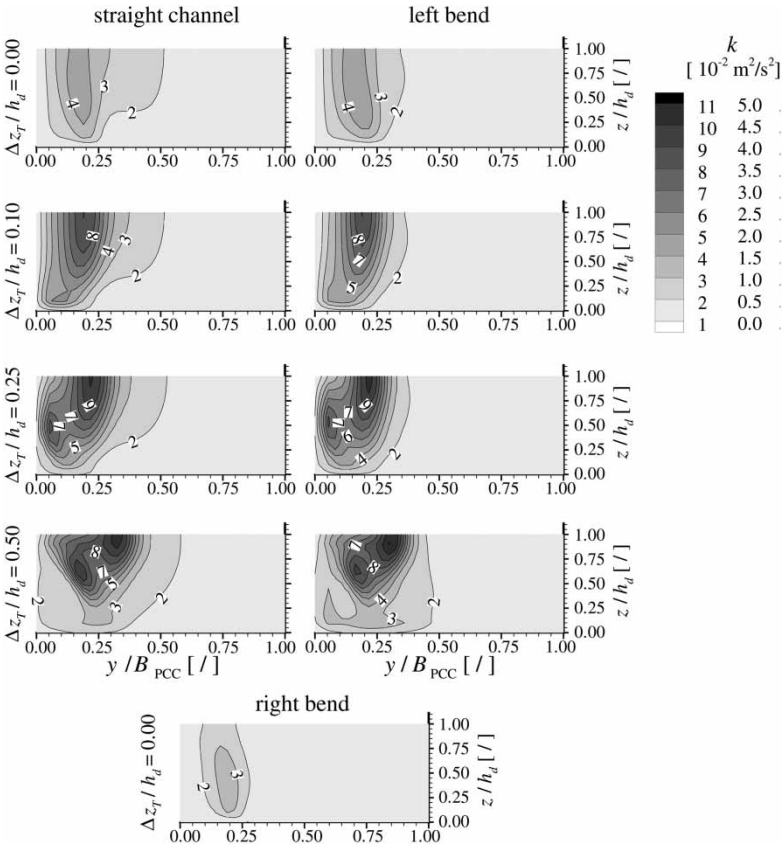

Figure 12 | Influence of difference in bed elevations on the cross-sectional distributions of the TKE in the CHZ (cross-section $x/B_{PCC} = -1.33$) for the confluences with the SC and with the LB in the tributary and influence of the RB in the CB' confluence.

the tributary have the opposite effect on the k_{max}. The presence of the RB induces reduction, while the presence of the LB induces an increase in k_{max}. The amount of reduction/increase is approximately the same for the two cases and ranges between 8 and 26%.

Effect of bed elevation discordance

To study the effect of an elevated tributary canal bed on the confluence hydrodynamics, numerical simulation results for the SC confluences with three $\Delta z_T/h_d$ values (0.10, 0.25, 0.50) are compared to the SC CB' case ($\Delta z_T/h_d = 0.00$) from the previous subsection.

Flow angles

Distributions of the δ and φ angles along the junction lines are presented in Figures 13(a) and 13(b). As can be seen, deflection of the flow angle δ from the junction angle α decreases with the increasing difference in bed elevations between the two canals (Figure 13(a)). This can be expected since the tributary flow for a given D_R value becomes stronger with increasing bed elevation discordance. Again, the greatest δ-angle deflections from the junction angle and the greatest differences between the four cases are present close to the bottom. Here, the δ-angle for $\Delta z_T/h_d = 0.50$ exceeds the value for the CB' case 1.3 to approximately four times. In the remaining two cases, $\Delta z_T/h_d = \{0.10, 0.25\}$, δ-angle increases by 15–166% and 6–80%, respectively. With distance from the tributary bottom, the difference from the CB' case becomes almost negligible for $\Delta z_T/h_d \leq 0.10$, except in the flow stagnation zone, close to the upstream junction corner; for $\Delta z_T/h_d > 0.25$ δ-angle distributions become almost uniform along 90% of the junction line (for $\Delta z_T/h_d = 0.50$ δ-angle varies between 65° and 70°).

As for the flow deflection in the vertical plane, it is worth noting that for $\Delta z_T/h_d > 0.10$, the φ-angle does not change the

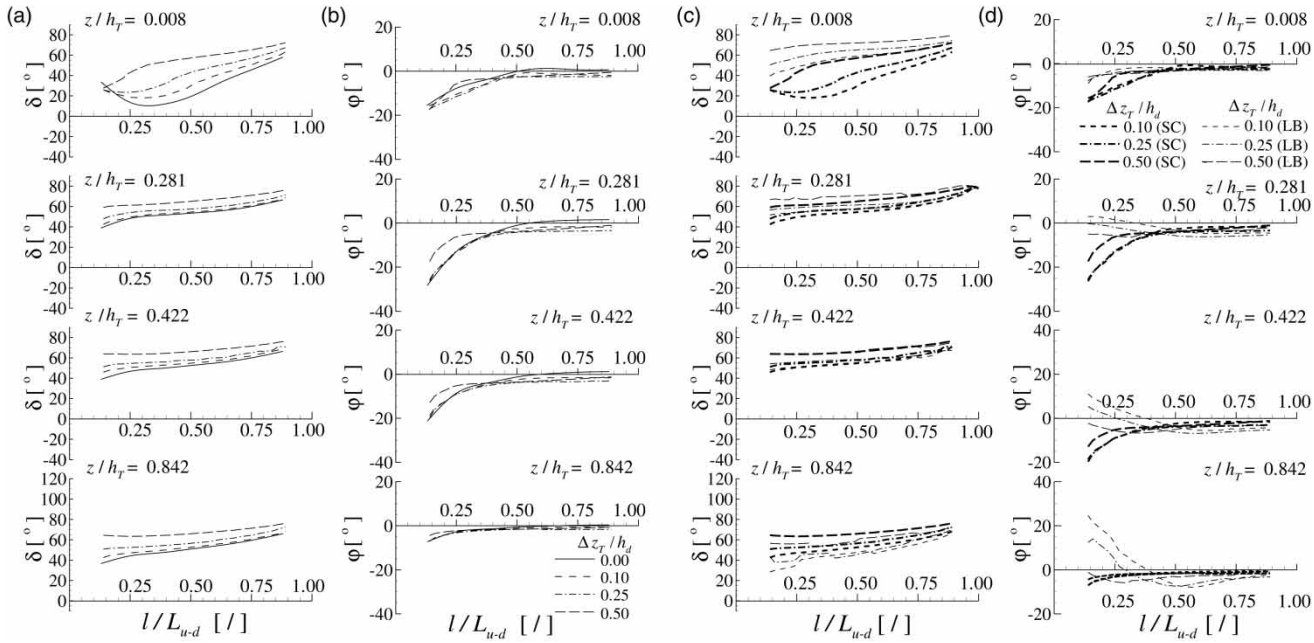

Figure 13 | (a) and (b) Effect of bed elevation discordance (Δz_T) on the distributions of flow angles along the junction lines at different elevations above the tributary bed; (c) and (d) combined effect of Δz_T and the upstream bend. Variations of δ-angle are presented on plots (a) and (c), and those of φ-angle on plots (b) and (d).

sign between the junction corners (Figure 13(b)), i.e., it is always negative, meaning that the flow is directed downwards. This is logical, as there is sudden expansion of tributary flow in the vertical direction at the backward facing step. Another interesting observation is that the 3D flow is less pronounced above $0.25h_T$ for $\Delta z_T/h_d = 0.50$ than for the other three cases. This can be attributed to the much stronger flow in the shallower tributary than that that enters the confluence from the deeper tributary canal.

Recirculation zone

It is important to notice that there are no conditions for the development of RZ at elevations below the tributary bed (Figures 14, 15(a) and 15(b)) in the DB' confluences. For $z < z_T$, the flow from the main canal skirts the area where tributary flow enters the main canal, which is consistent with the experimental observations of Biron *et al.* (1996b). This skirting is a consequence of very strong downward tributary flow. Unlike the CB' case, where RZ exists from the very bottom of the tributary canal, development of RZ above the tributary bed is postponed (Figures 14, 15(a) and 15(b)). For $\Delta z_T/h_d \leq 0.25$ RZ development starts $0.15h_d$ above the tributary bed, whereas for $\Delta z_T/h_d = 0.50$ the postponement interval increases to $0.20h_d$ (Figures 15(a) and 15(b)). In contrast to the CB' case (Figure 14, case 1), in which the longitudinal axis of the RZ is parallel with the walls, in the DB' cases the axes are inclined at an angle to the sidewall (Figures 14 and 15(c)). The greater the difference in bed elevations Δz_T, the greater the inclination angle β. After initial increase, the β-angle-value decreases with distance from the bottom regardless of the Δz_T-value. For $\Delta z_T/h_d \leq 0.10$, RZ axis becomes parallel to the wall starting from $0.65h_d$. Apart from a consistent decrease in the RZ length with an increase in Δz_T (Figure 15(a)) and development of an additional vortex due to strong shear in case 5 ($\Delta z_T/h_d = 0.25$) for $z \geq 0.70h_d$ (Figure 14), it is important to note that the structure of the RZ is destroyed close to the water surface when $\Delta z_T/h_d \geq 0.25$ (Figures 15(a), 15(b) and 15(c)). The destruction can be attributed to strong 3D flow in the upper layers (i.e., large vertical velocity component w, which is of the same order of magnitude as the horizontal velocity $V_{xy} = \sqrt{u^2 + v^2}$ – Figure 16). However, for $\Delta z_T/h_d \leq 0.10$, RZ exists up to the free surface. Although 40% shorter, the zone is 9% wider than that in the CB' case (case 1). Sudden increase in RZ width above $0.80h_d$ for $\Delta z_T/h_d = 0.25$ results from the additional vortex development. Thus, the RZ width exceeds those developed in cases 1 and 4 by 18 and 27%, respectively.

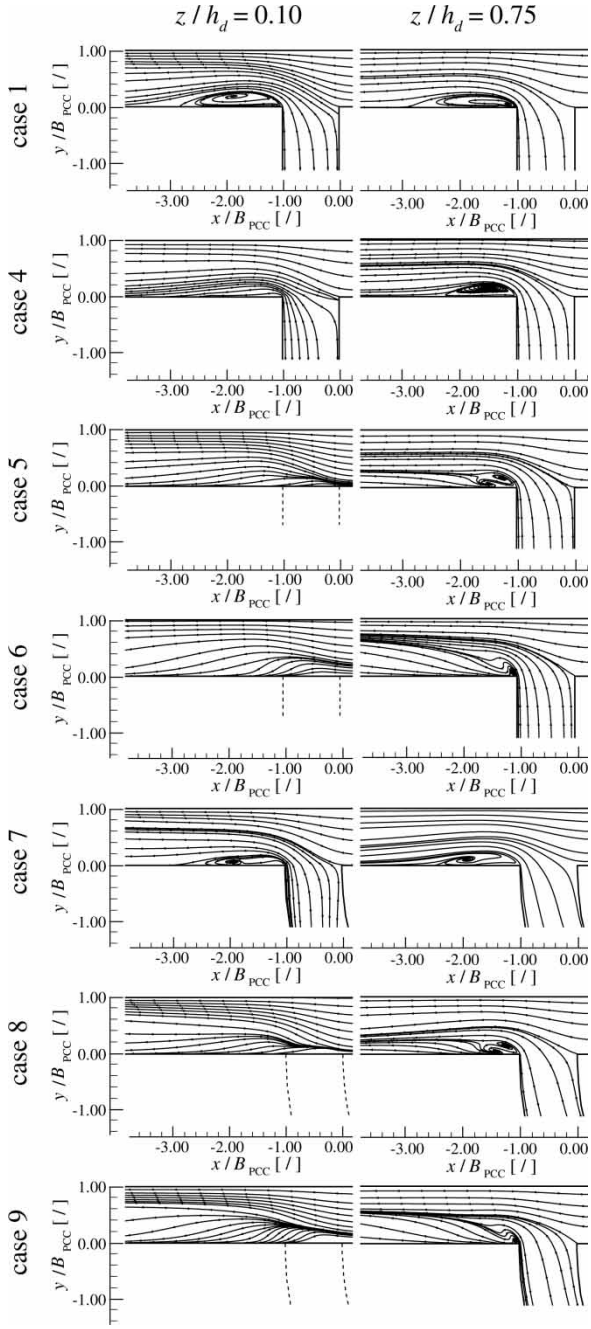

Figure 14 | Effect of bed elevation discordance and combined effect of the two controls on the evolution of the RZ throughout the flow depth. Description of the cases is given in Table 1.

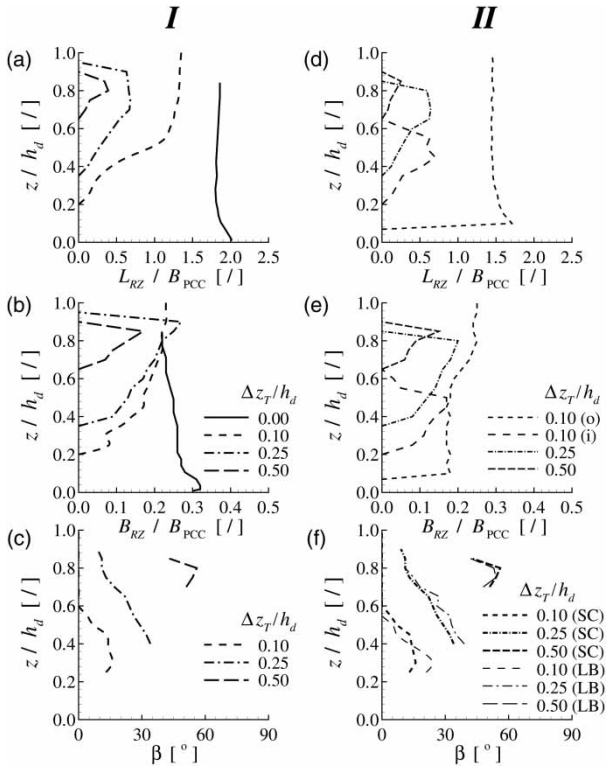

Figure 15 | Variations of the RZ length, maximal width and inclination angle throughout the flow depth. (a), (b) and (c) Effect of bed elevation discordance; (d), (e) and (f) combined effect of Δz_T and the upstream bend. Variations of the non-dimensional RZ length are presented on plots (a) and (d), variations of the non-dimensional RZ maximal width on plots (b) and (e), and variations of the inclination angle on plots (c) and (f).

Reduction of the RZ size and loss of its strength with an increase in Δz_T is also visible on the cross-sectional distributions of the stream-wise (u) and vertical (w) velocity distributions (Figure 16). The area with the backward flow is moved from the bottom (in the CB' case – $\Delta z_T/h_d = 0.0$) to the layers above the tributary bed ($\Delta z_T/h_d > 0.0$ – u-velocity distributions). Moreover, it is gradually shifted from the side-wall towards the main canal axis with an increase in Δz_T, indicating the above-mentioned change in orientation of the RZ on the horizontal plane. Reduction in the u-velocity magnitude and the size of the core with u_{max}, with an increase in Δz_T is accompanied with an increase in the w-velocity, whose order of magnitude reaches that of the velocity V_{xy}, and the enlargement of the cores with the maximal upward and downward velocities (Figure 16(b)). For $\Delta z_T/h_d = 0.50$, the area of strong 3D flow occupies almost $0.50B$. The greatest w-velocity magnitudes are present in the subsurface layer, which explains the destruction of the RZ.

TKE

As expected, bed elevation discordance affects both k-distributions and k_{max}-values (Figure 12, straight channel

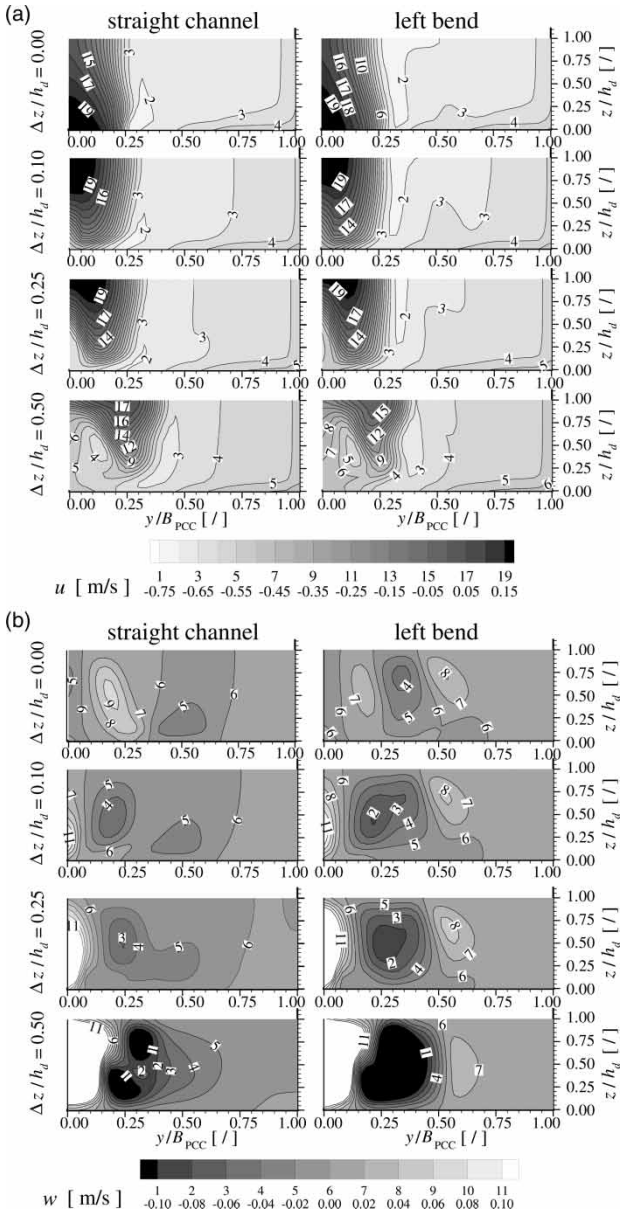

Figure 16 | Influence of difference in bed elevations on the cross-sectional distributions of the stream-wise (u) and vertical (w) velocities in the CHZ (cross-section $x/B_{PCC} = -1.33$) for the confluences with the straight tributary channel and with the LB in the tributary.

column). The core of k_{max} is lifted above the tributary bed and k_{max} is increased by {116, 145, 155}% for $\Delta z_T/h_d = \{0.10, 0.25, 0.50\}$, respectively. Moreover, when $\Delta z_T/h_d \geq 0.25$, the k_{max}-core is split into two smaller ones, one on each side of the detached inclined RZ. The high k-intensities decrease rapidly – by $x/B_{PCC} \approx -2.00$ the k_{max} drops below the k_{max}-value for the CB' confluence. This is in accordance with the rapid reduction of the RZ length.

Combined effect of the left bend and bed elevation discordance

The combined effect of the two controls is investigated by comparison of the numerical simulation results for SC confluences with DB from the previous subsection with those for the DB' confluences that have a LB in the tributary (Figure 2(a)).

Flow angles

As with the CB' confluences analysed in the first subsection, the presence of the LB in a tributary results in a reduced deflection of the δ-angle from the junction angle α in the bottom layers (Figure 13(c)). The effect of LB decreases with an increase in Δz_T. For $\Delta z_T/h_d = 0.10$, the effect of LB is equivalent to the increase in Δz_T to $0.50h_d$ (Figures 13(a) and 13(c)). The maximal increase in δ is 190%. For $\Delta z_T/h_d = \{0.25, 0.50\}$, the increase is ≈125%. The change in dominance between the centrifugal force from the LB and that which develops due to change in the tributary flow direction, happens at $z \approx 0.40h_T$ for all Δz_T-values, in contrast to $z \approx 0.50h_T$ for the CB' case. Again, above this characteristic level, the flow from the tributary starts turning more rapidly under the influence of the main canal flow. Irregularities in the δ-angle distributions, that are observed in the subsurface layers (Figure 13(c), $z/h_T = 0.842$) should be further investigated as they are not present in the DB' confluences of channels with higher B/h ratio (i.e., for $B/h \approx 20$, Đorđević 2010b).

The effect of LB on the change in the vertical flow direction between the two junction corners is postponed with the increase in Δz_T. For $\Delta z_T/h_d = 0.10$, the change begins at $\approx 0.25h_T$, for $z_T/h_d = 0.25$, at $\approx 0.40h_T$, whereas for $z_T/h_d = 0.50$, the φ-angle is always negative, i.e., the flow is always directed towards the bottom. In addition, the place on the junction line where the φ-angle changes its sign moves upstream as the Δz_T increases. For $\Delta z_T/h_d = 0.10$, the change of sign happens at $0.35L_{u\text{-}d}$, while for $\Delta z_T/h_d = 0.25$, it happens at $\approx 0.25L_{u\text{-}d}$ (Figure 13(d)).

Recirculation zone

Generally, two distinct Δz_T-ranges can be distinguished: $\Delta z_T/h_d \leq 0.10$ and $\Delta z_T/h_d \geq 0.25$. For $\Delta z_T/h_d \leq 0.10$, influence of the LB is dominant in the bottom layers. This explains development of the RZ with an axis parallel to the sidewall at $z = \Delta z_T$ (Figure 14, case 7), which is not present when there is no bend in the tributary (Figure 14, case 4). The influence of bed elevation discordance begins from $0.25h_d$ (not presented in Figure 14). The resulting RZ is 10–20% longer and 6–14% wider than that in case 4, due to interaction of the two controls.

For $\Delta z_T/h_d \geq 0.25$, the shape of the curves describing variations in RZ length and maximal width in the CHZ of the confluences with LB in the tributary (Figures 15(d) and 15(e)), essentially remains unaltered when compared to the confluences of two straight canals (Figures 15(a) and 15(b)). In the LB confluences, RZ becomes narrower and shorter (for $\Delta z_T/h_d = 0.25$ the length is reduced by 6% and width by 30%, while for $\Delta z_T/h_d = 0.50$, these reductions are 65% for the length and 11% for the width). However, no rule can be established, yet, for the change in the RZ inclination angle due to combined influence of the two controls (Figures 15(c) and 15(f)).

Reduction of the RZ width due to the presence of the LB is also noticeable in the cross-sectional u-velocity distributions (Figure 16(a), $\Delta z_T/h_d \geq 0.10$). As can be seen, the core of the backward velocity close to the left sidewall is lifted towards the free surface by $0.05h_d$ and isovels are almost vertical lines (Figure 16(a), column 'left bend', $\Delta z_T/h_d = \{0.10, 0.25\}$) when compared to corresponding cases in the column 'straight channel'. The resulting increase in shear is 12 and 14% for $\Delta z_T/h_d = \{0.10, 0.25\}$, respectively. Influence of the LB reduces gradually with the increase in Δz_T. For $\Delta z_T/h_d = 0.50$, it is almost negligible and the shear is reduced by 14%. The presence of the LB also increases upward maximal velocities (Figure 16(b)) by {4.3, 8.3, 15.6}% for $\Delta z_T/h_d = \{0.10, 0.25, 0.50\}$, respectively. The respective increases in the maximal downward velocity are {41.4, 55.7, 17.8}%.

TKE

The influence of Δz_T on the k-distributions and k_{max} in the LB confluences is similar to that in the SC confluences (Figure 12). The increase in k_{max} is {103, 140, 150}% for $\Delta z_T/h_d = \{0.10, 0.25, 0.50\}$, respectively. Comparison of the SC and LB distributions for the fixed $\Delta z_T/h_d$-value reveals that in the LB case the zone of high k-values is confined to the part of the cross-section on the tributary side ($y/B_{PCC} < 0.50$). Additionally, the percentage of increase in k_{max} due to the presence of the LB lowers with the increasing Δz_T (for $\Delta z_T = 0.10h_d$ k_{max}-value increases by 4–8%, for $\Delta z_T = 0.25h_d$ the increase is 1.3–4%). The presence of the LB in the case of $\Delta z_T = 0.50h_d$ has quite the opposite effect on k_{max}-values – they are reduced by 10–17%. This changing influence of the LB requires further investigation.

CONCLUSIONS

The effects of upstream planform curvature and bed elevation discordance between the tributary and main canals on the confluence hydrodynamics were studied using the 3D finite-volume numerical model. Nine combinations of three possible confluence planforms (confluence with the SC, confluence with the RB and confluence with the LB in a tributary) and four chosen values of bed elevation discordance $\Delta z_T/h_d = \{0.00, 0.10, 0.25, 0.50\}$ (where 0.00 value pertains to the CB' confluence and the value of 0.5 is the maximal observed value in field confluences) were analysed. Comparison of the numerical simulation results led to the following conclusions:

1. The upstream planform curvature can be added to the list of major controls to the confluence hydrodynamics only if the outer bank of the upstream bend ends in the downstream junction corner.
2. Turning of the tributary flow under the influence of the main canal flow becomes slower and less pronounced with an increasing difference in bed elevations between the two canals. Additionally, 3D flow effects are localised to the narrow zone close to the upstream junction corner where the two flows collide and the bottom layers where tributary flow expands in the vertical direction due to the presence of the backward facing step in the bed of the tributary canal.
3. Although almost 2D, at the tributary entrance to the confluence, the flow in the post-confluence canal becomes 3D. The strength of the 3D flow enhances with an

increase in $\Delta z_T/h_d$ due to larger pressure gradients close to the downstream junction corner, i.e., w_{max} is increased approximately two times for $\Delta z_T/h_d = 0.10$, five times for $\Delta z_T/h_d = 0.25$ and up to eight times for $\Delta z_T/h_d = 0.50$, thus attaining the same order of magnitude as the horizontal velocity.

4. Enhanced 3D flow close to the sidewall shifts the RZ away from the wall to the boundary streamline that issues from the downstream junction corner, thus changing the RZ orientation whose axis becomes inclined at an angle to the wall. Additionally, the size of the zone (its length and width) is reduced. The greater the difference Δz_T, the greater the RZ size reduction and the greater the RZ inclination angle.
5. For higher $\Delta z_T/h_d$ values ($\Delta z_T/h_d > 0.25$), structure of the RZ is completely destroyed close to the free surface, where the core of the w_{max} is located.
6. The presence of an upstream bend, whose outer bank ends in the downstream junction corner, additionally enhances 3D flow and reduces the size of RZ at DB' confluences. In confluences with $\Delta z_T/h_d \geq 0.25$, the effect of bed elevation discordance on the RZ size variations is dominant throughout the flow depth. On the other hand, in the confluences with $\Delta z_T/h_d \leq 0.10$, where 3D flow effects are less pronounced, the effect of the bend dominates up to $0.25h_d$. Above this level, the two controls start to interact.
7. Difference in bed elevations between the tributary and main canals increases TKE by 100–150% regardless of the confluence platform. However, the combined effect of Δz_T and the LB needs further investigation.

REFERENCES

Best, J. L. & Reid, I. 1984 Separation zone at open-channel junctions. *J. Hydraul. Eng.* **110** (11), 1588–1594.

Best, J. L. & Roy, A. G. 1991 Mixing-layer distortion at the confluence of channels of different depth. *Nature* **350**, 411–413.

Biron, P. M. & Lane, S. N. 2008 Modelling hydraulics and sediment transport at river confluences. In: *River Confluences, Tributaries and the Fluvial Network* (S. P. Rice, A. G. Roy & B. L. Rhoads, eds). Wiley, Chichester, UK, pp. 17–38.

Biron, P., Roy, A. G., Best, J. L. & Boyer, C. J. 1993 Bed morphology and sedimentology at the confluence of unequal depth channels. *Geomorphology* **8**, 115–129.

Biron, P., Roy, A. G. & Best, J. L. 1996a Turbulent flow structure at concordant and discordant open-channel confluences. *Exp. Fluids* **21**, 437–446.

Biron, P., Best, J. L. & Roy, A. G. 1996b Effects of bed discordance on flow dynamics at open-channel confluences. *J. Hydraul. Eng.* **122** (12), 676–682.

Biron, P. M., Ramamurthy, A. S. & Han, S. 2004 Three-dimensional numerical modeling of mixing at river confluences. *J. Hydraul. Eng. ASCE* **130** (3), 243–253.

Bradbrook, K. F., Biron, P., Lane, S. N., Richards, K. S. & Roy, A. G. 1998 Investigation of controls on secondary circulation in a simple confluence geometry using a three-dimensional numerical model. *Hydrol. Process.* **12**, 1371–1396.

Bradbrook, K. F., Lane, S. N. & Richards, K. S. 2000a Numerical simulation of the three-dimensional, time-averaged flow structure at river channel confluences. *Water Resour. Res.* **36** (9), 2731–2746.

Bradbrook, K. F., Lane, S. N., Richards, K. S., Biron, P. M. & Roy, A. G. 2000b Large eddy simulation of periodic flow characteristics at river channel confluences. *J. Hydraul. Res.* **38** (3), 207–215.

Bradbrook, K. F., Lane, S. N., Richards, K. S., Biron, P. M. & Roy, A. G. 2001 Role of bed discordance at asymmetrical river confluences. *J. Hydraul. Eng.* **127** (5), 351–368.

Celik, I. B., Ghia, U., Roache, P. J., Freitas, C. J., Coleman, H. & Raad, P. E. 2008 Procedure for estimation and reporting of uncertainty due to discretization in CFD applications. *ASME J. Fluids. Eng.* **130**, 1–4.

De Serres, B., Roy, A. G., Biron, P. M. & Best, J. L. 1999 Three-dimensional structure of flow at a confluence of river channels with discordant beds. *Geomorphology* **26**, 313–335.

Đorđević, D. 2010a Numerical simulation of 3D flow at right-angled confluence with and without upstream planform curvature. *Proceedings of the 9th International Conference on Hydroinformatics – HIC2010*, Tianjin, China, **Vol. 1**, pp. 299–307.

Đorđević, D. 2010b Numerical Investigation of River Confluence Hydrodynamics. PhD Thesis, Faculty of Civil Engineering, University of Belgrade, Belgrade, 381 pp.

Đorđević, D. 2012 Application of 3D numerical models in confluence hydrodynamics modelling. *Proceedings of the XIX International Conference on Computational Methods in Water Resources*, Urbana, USA. Available from: http://cmwr2012.cee.illinois.edu/HighDimCompModelingRiversStreams(Proceedings).html.

Đorđević, D. (in preparation) Performance of k-ε type turbulence models in confluence hydrodynamics modelling.

Đorđević, D. & Biron, P. M. 2008 Role of upstream planform curvature at asymmetrical confluences – laboratory experiment revisited. *Proceedings of the 4th International Conference on Fluvial Hydraulics – River Flow 2008*, Cesme, Turkey, Vol. **3**, pp. 2277–2286.

Đorđević, D. & Ivetić, M. 2006 Numerical modelling of three-dimensional flow at the confluence of Sava and Danube Rivers. *Proceedings of the 7th International Conference on Hydroinformatics – HIC 2006*, Nice; 2: pp. 1147–1154.

Đorđević, D. & Jovanović, M. 2006 On the effect of the bed morphology on the river confluence hydrodynamics. *Proceedings of the 3rd International Conference on Fluvial Hydraulics – River Flow 2006*, Lisbon; 2: pp. 1165–1174.

Gaudet, J. M. & Roy, A. G. 1995 Effect of bed morphology on flow mixing length at river confluences. *Nature* **373**, 138–139.

Gurram, S. K., Karki, K. S. & Hager, W. H. 1997 Subcritical junction flow. *J. Hydraul. Eng. ASCE* **123** (5), 447–455.

Hager, W. H. 1987 Discussion of 'Separation zone at open-channel junctions'. *J. Hydraul. Eng. ASCE* **113** (4), 539–543.

Hager, W. H. 1989 Transitional flow in channel junctions. *J. Hydraul. Eng. ASCE* **115** (2), 243–259.

Hsu, C. C., Wu, F. S. & Lee, W. J. 1998a Flow at 90° equal-width open-channel junction. *J. Hydraul. Eng. ASCE* **124** (2), 186–191.

Hsu, C. C., Lee, W. J. & Chang, C. H. 1998b Subcritical open-channel junction flow. *J. Hydraul. Eng. ASCE* **124** (8), 847–855.

Huang, J., Weber, L. J. & Lai, Y. G. 2002 Three-dimensional study of flows in open-channel junctions. *J. Hydraul. Eng. ASCE* **128** (3), 268–280.

Lane, S. N., Biron, P. M., Bradbrook, K. F., Butler, J. B., Chandler, J. H., Crowell, M. D., McLelland, S. J., Richards, K. S. & Roy, A. G. 1998 Three-dimensional measurement of river channel flow processes using Acoustic Doppler Velocimetry. *Earth Surf. Process. Landf.* **23**, 1247–1267.

Lane, S. N., Bradbrook, K. F., Richards, K. S., Biron, P. M. & Roy, A. G. 2000 Secondary circulation cells in river channel confluences: measurement artefacts or coherent flow structures? *Hydrol. Process.* **14**, 2047–2071.

Lane, S. N., Bradbrook, K. F., Richards, K. S., El-Hames, A., Biron, P. M. & Roy, A. G. 1999 The application of computational fluid dynamics to natural river channels: three-dimensional versus two-dimensional approaches. *Geomorphology* **29** (1–2), 1–20.

Mosley, M. P. 1976 An experimental study of channel confluences. *J. Geol.* **94**, 535–562.

Olsen, N. R. 2000 *CFD Algorithms for Hydraulic Engineering*. The Norwegian University of Science and Technology, Trondheim, Norway.

Olsen, N. R. 2003 Three-dimensional CFD modeling of self-forming meandering channel. *J. Hydraul. Eng. ASCE* **129** (5), 366–372.

Ramamurthy, A. S., Carballada, L. B. & Tran, D. M. 1988 Combining open channel flow at right-angled junctions. *J. Hydraul. Eng. ASCE* **114** (12), 1449–1460.

Rhoads, B. L. & Kenworthy, S. T. 1995 Flow structure at an asymmetrical stream confluence. *Geomorphology* **11**, 273–293.

Rhoads, B. L. & Kenworthy, S. T. 1998 Time-averaged flow structure in the central region of a stream confluence. *Earth Surf. Process. Landf.* **23** (2), 171–191.

Rhoads, B. L. & Kenworthy, S. T. 1999 On secondary circulation, helical motion and Rozovski-based analysis of time-averaged two-dimensional velocity fields at confluences. *Earth Surf. Process. Landf.* **24** (4), 369–375.

Rhoads, B. L. & Sukhodolov, A. N. 2001 Field investigation of the three-dimensional flow structure at stream confluences: 1. Thermal mixing and time-averaged velocities. *Water Resour. Res.* **37** (9), 2393–2410.

Rhoads, B. L. & Sukhodolov, A. N. 2004 Spatial and temporal structure of shear layer turbulence at a stream confluence. *Water Resour. Res.* **40**, W06304.

Rhoads, B. L. & Sukhodolov, A. N. 2008 Lateral momentum flux and the spatial evolution of flow within a confluence mixing interface. *Water Resour. Res.* **44**, W08440.

Rüther, N. & Olsen, N. R. 2006 3D modelling of transient bed deformation in a sine-generated laboratory channel with two different width to depth ratios. *Proceedings of the 3rd International Conference on Fluvial Hydraulics – River Flow 2006*, Lisbon; 2: pp. 1269–1275.

Shakibainia, A., Tabatabai, M. R. M. & Zarrati, A. R. 2010 Three-dimensional numerical study of flow structure in channel confluences. *Can. J. Civ. Eng.* **37**, 772–781.

Shumate, E. D. & Weber, L. J. 1998 Experimental description of combining flows at an open-channel junction. *Proceedings of the International Water Resources Engineering Conference*, Memphis, pp. 1679–1684.

Stoesser, T., Rüther, N. & Olsen, N. R. 2010 Calculation of primary and secondary flow and boundary shear stresses in a meandering channel. *Adv. Water Resour.* **33**, 158–170.

Sukhodolov, A. N. & Rhoads, B. L. 2001 Field investigation of the three-dimensional flow structure at stream confluences: 2. Turbulence. *Water Resour. Res.* **37** (9), 2411–2424.

Viscardi, J. M., Pujol, A., Weitbrecht, V., Jirka, G. H. & Olsen, N. R. 2006 Numerical simulations on the Parana de las Palmas River. *Proceedings of the 3rd International Conference on Fluvial Hydraulics – River Flow 2006*, Lisbon; 1: pp. 367–377.

Weerakoon, S. B. & Tamai, N. 1989 Three-dimensional calculation of flow in river confluences using boundary-fitted coordinates. *J. Hydrosci. Hydraul. Eng.* **7** (1), 51–62.

Weerakoon, S. B., Tamai, N. & Kawahara, Y. 1990 Bed topography, bed shear stress distribution and velocity field in a confluence. *Proc. Hydraul. Eng. JSCE*, **34**, 307–312.

Yakhot, V., Orszag, S. A., Thangam, S., Gatski, T. B. & Speciale, C. G. 1992 Development of turbulence models for shear flows by double expansion technique. *Phys. Fluids A* **4** (4), 1510–1520.

First received 25 October 2011; accepted in revised form 28 September 2012. Available online 8 November 2012